Astrocytes Control Breathing Through pH-Dependent Release of ATP

Alexander V. Gourine, *et al.*

Science **329**, 571 (2010);
DOI: 10.1126/science.1190721

development of human prostatic tissue (fig. S5). Results were reproducible for four independent patient samples and showed little variation between replicate grafts.

We next introduced a lentivirus carrying both activated (myristoylated) AKT and ERG (*7*) into primary basal and luminal cells (Fig. 2A). After 8 to 16 weeks in vivo, we observed the development of abnormal structures expressing AKT, nuclear ERG, and the fluorescently linked marker RFP (Fig. 2, B and D) from primary basal cells but not luminal cells (Fig. 2B). Structures lacking RFP expression, indicating an absence of lentiviral infection, were benign, demonstrating the requirement for expression of oncogenes to initiate a malignant phenotype. We observed an expansion of AR^+ luminal-like cells with retention of the $p63^+$ basal layer in basal cell–derived lesions (Fig. 2C). In many areas, cells were positive for both PSA and AMACR (Fig. 2C), a marker of both high-grade PIN and prostate cancer (*24*). Based on the presence of morphologically malignant AR^+/PSA^+ luminal cells surrounded by $p63^+$ basal cells, basal cell–derived lesions fulfill the histological criteria for the diagnosis of high-grade PIN, the precursor lesion to invasive prostate cancer (*25*).

We evaluated whether additional genetic alterations could be used to recapitulate human prostate cancer. Primary cells were transduced with the RFP-marked lentivirus carrying AKT and ERG and a green fluorescent protein (GFP)–marked lentivirus carrying AR (*26*) (Fig. 3A). Combination of AKT, ERG, and AR resulted in the development of adenocarcinoma from basal cells (Fig. 3B) but not luminal cells. Although some basal cell–derived structures retained expression of p63 and resembled PIN (fig. S6), many glands had lost the basal layer (Fig. 3B and fig. S6), a defining histological feature used by pathologists for the diagnosis of human prostate cancer (*11*). Cancerous glands expressed PSA (Fig. 3B and fig. S7), AR, and AMACR (Fig. 3B) in patterns indistinguishable from those in patient samples of clinical prostate cancer (Fig. 3C). At high power, cells from cancer lesions exhibited hyperchromatic nuclei with visible nucleoli [Fig. 3, B and C, hematoxylin and eosin (H&E) insets]. Clinical prostate cancer presents as a multifocal disease with considerable heterogeneity of disease grade (*2*). Within the same grafts, we observed lesions that correspond to benign structures ($AR^+/PSA^+/p63^+/AMACR^-$), PIN ($AR^+/PSA^+/p63^+/AMACR^+$), and cancer ($AR^+/PSA^+/p63^-/AMACR^+$), recapitulating the mixed histology found in cancer patients (fig. S6).

Cells within the basal fraction can regenerate benign prostate tissue in immunodeficient mice. Introduction of oncogenic alterations in the target cells can induce a disease that mimics human prostate cancer, establishing basal cells as one cell of origin for prostate cancer. Our results support studies in the mouse demonstrating that histological characterization of cancers in the absence of functional studies can be misleading for determining cells of origin (*27*–*30*). As the human prostate epithelial hierarchy is further delineated, additional cell types may be identified with cancer-initiating properties.

Even though basal cells express low levels of AR, they share the property of androgen-independence (*31*) with late-stage castration-resistant prostate cancer cells (*8*), suggesting that pathways involved in basal cell function and self-renewal may play a role in tumor cell survival and disease recurrence after androgen withdrawal. Therefore, further investigation of target cells may provide insight into treatments for castration-resistant prostate cancer.

References and Notes

1. K. J. Pienta *et al.*, *Prostate* **68**, 629 (2008).
2. E. T. Ruijter, C. A. van de Kaa, J. A. Schalken, F. M. Debruyne, D. J. Ruiter, *J. Pathol.* **180**, 295 (1996).
3. M. Yoshimoto *et al.*, *Cancer Genet. Cytogenet.* **169**, 128 (2006).
4. S. A. Tomlins *et al.*, *Science* **310**, 644 (2005).
5. B. S. Carver *et al.*, *Nat. Genet.* **41**, 619 (2009).
6. J. C. King *et al.*, *Nat. Genet.* **41**, 524 (2009).
7. Y. Zong *et al.*, *Proc. Natl. Acad. Sci. U.S.A.* **106**, 12465 (2009).
8. C. D. Chen *et al.*, *Nat. Med.* **10**, 33 (2004).
9. H. Okada *et al.*, *Virchows Arch. A Pathol. Anat. Histopathol.* **421**, 157 (1992).
10. J. K. Parsons, W. R. Gage, W. G. Nelson, A. M. De Marzo, *Urology* **58**, 619 (2001).
11. K. J. Wojno, J. I. Epstein, *Am. J. Surg. Pathol.* **19**, 251 (1995).
12. X. Ma *et al.*, *Cancer Res.* **65**, 5730 (2005).
13. X. Wang *et al.*, *Nature* **461**, 495 (2009).
14. T. Iwata *et al.*, *PLoS ONE* **5**, e9427 (2010).
15. D. A. Lawson *et al.*, *Proc. Natl. Acad. Sci. U.S.A.* **107**, 2610 (2010).
16. D. J. Mulholland *et al.*, *Cancer Res.* **69**, 8555 (2009).
17. S. Wang *et al.*, *Proc. Natl. Acad. Sci. U.S.A.* **103**, 1480 (2006).
18. N. Barker *et al.*, *Nature* **457**, 608 (2009).
19. A. P. Verhagen *et al.*, *Cancer Res.* **52**, 6182 (1992).
20. A. S. Goldstein *et al.*, *Proc. Natl. Acad. Sci. U.S.A.* **105**, 20882 (2008).
21. I. P. Garraway *et al.*, *Prostate* **70**, 491 (2010).
22. W. C. Hahn *et al.*, *Nature* **400**, 464 (1999).
23. E. Quintana *et al.*, *Nature* **456**, 593 (2008).
24. C. L. Wu *et al.*, *Hum. Pathol.* **35**, 1008 (2004).
25. J. E. McNeal, D. G. Bostwick, *Hum. Pathol.* **17**, 64 (1986).
26. L. Xin *et al.*, *Proc. Natl. Acad. Sci. U.S.A.* **103**, 7789 (2006).
27. K. K. Youssef *et al.*, *Nat. Cell Biol.* **12**, 299 (2010).
28. E. Passegué, E. F. Wagner, I. L. Weissman, *Cell* **119**, 431 (2004).
29. C. W. So *et al.*, *Cancer Cell* **3**, 161 (2003).
30. A. Cozzio *et al.*, *Genes Dev.* **17**, 3029 (2003).
31. H. F. English, R. J. Santen, J. T. Isaacs, *Prostate* **11**, 229 (1987).

32. We thank B. Anderson for manuscript preparation; D. Cheng for cell sorting; Y. Zong for vectors; H. Zhang for tissue preparation; and A. Chhabra, B. Van Handel, D. Mulholland, C. Soroudi, and T. Stoyanova for discussion and technical help. A.S.G. is supported by an institutional Ruth L. Kirschstein National Research Service Award (GM07185). J.H. is supported by the American Cancer Society, the Department of Defense (DOD) Prostate Cancer Research Program, and the UCLA SPORE in Prostate Cancer (principal investigator, R. Reiter). I.P.G is supported by the DOD and the Jean Perkins Foundation. O.N.W. is an Investigator of the Howard Hughes Medical Institute. J.H., I.P.G., and O.N.W. are supported by a Challenge Award from the Prostate Cancer Foundation.

Supporting Online Material

www.sciencemag.org/cgi/content/full/329/5991/568/DC1
Materials and Methods
Figs. S1 to S7
Table S1
References

23 March 2010; accepted 24 June 2010
10.1126/science.1189992

Astrocytes Control Breathing Through pH-Dependent Release of ATP

Alexander V. Gourine,[1]* Vitaliy Kasymov,[1] Nephtali Marina,[1] Feige Tang,[2] Melina F. Figueiredo,[2] Samantha Lane,[2] Anja G. Teschemacher,[2] K. Michael Spyer,[1] Karl Deisseroth,[3] Sergey Kasparov[2]*

Astrocytes provide structural and metabolic support for neuronal networks, but direct evidence demonstrating their active role in complex behaviors is limited. Central respiratory chemosensitivity is an essential mechanism that, via regulation of breathing, maintains constant levels of blood and brain pH and partial pressure of CO_2. We found that astrocytes of the brainstem chemoreceptor areas are highly chemosensitive. They responded to physiological decreases in pH with vigorous elevations in intracellular Ca^{2+} and release of adenosine triphosphate (ATP). ATP propagated astrocytic Ca^{2+} excitation, activated chemoreceptor neurons, and induced adaptive increases in breathing. Mimicking pH-evoked Ca^{2+} responses by means of optogenetic stimulation of astrocytes expressing channelrhodopsin-2 activated chemoreceptor neurons via an ATP-dependent mechanism and triggered robust respiratory responses in vivo. This demonstrates a potentially crucial role for brain glial cells in mediating a fundamental physiological reflex.

The role of astrocytes in the brain is by no means limited to just providing structural and metabolic support to neurons. Astrocytes are closely associated with cerebral blood vessels and are thought to regulate cerebrovascular tone, adjusting blood supply to match

local metabolic demands (*1*–*6*). A single astrocyte may enwrap several neuronal somata (*7*) and make contact with thousands of synapses (*8*), potentially regulating synaptic strength and information processing (*4*, *9*–*14*). However, direct evidence demonstrating the functional role of astrocytes in complex behaviors is only now starting to emerge (*15*).

Astrocytes provide a vascular-neuronal interface and are in a position to quickly relay blood-borne stimuli to the activities of neuronal networks. Does this have a functional role in the detection of the relevant stimuli by brain chemosensors that monitor key homeostatic parameters, including glucose concentration, pH, and partial pressure of CO_2 (P_{CO_2})? Here, we tested the hypothesis that astrocytes residing within the respiratory chemoreceptor areas of the brainstem are functional respiratory pH sensors [supporting online material (SOM) text 2.1 and 2.2].

Because astrocytes are electrically nonexcitable but display Ca^{2+} excitability (reactive increases in cytosolic $[Ca^{2+}]_i$ concentration), we studied their behavior using genetically encoded Ca^{2+} indicator *Case12* (SOM text 1.3) (*16*, *17*). *Case12* was expressed in astrocytes residing at and near the classical chemosensitive area (*18*) of the ventral surface of the medulla oblongata (VS) of rats by using an adenoviral vector with enhanced shortened glial fibrillatory acidic protein (GFAP) promoter (figs. S1 and S2 and SOM text 1.3) (*19*).

In vivo, a 0.2 pH unit decrease on the VS of anesthetized and artificially ventilated rats ($n = 7$ rats) evoked an immediate increase in $[Ca^{2+}]_i$ across the field of astrocytes transduced with *Case12* (Fig. 1A and movie S1). Intracellular acidification reduces *Case12* fluorescence and may therefore mask the late phases of the response (SOM text 1.3 and 2.5). Prolonged and sustained astrocytic $[Ca^{2+}]_i$ responses were observed more laterally, at the level of the chemosensitive retrotrapezoid nucleus (RTN) (Fig. 1A). Subsequent histological examination of the chemoresponsive areas confirmed contacts of transduced astrocytes with pia mater and penetrating arterioles (fig. S3).

Propagating Ca^{2+} excitation of ventral medullary astrocytes in response to acidification was also observed in different in vitro preparations such as acute horizontal brainstem slices of adult rats ($n = 56$ slices) (Fig. 1, B and C, and movie S2), organotypic brainstem slice cultures ($n = 114$ slices) (Fig. 1E, fig. S4, and movie S3), and dissociated VS cell cultures ($n = 19$ cultures) (fig. S5). In brainstem slices of adult rats, in which blood vessels were visualized with lectin, many pH-sensitive astrocytes were found to be located adjacent to the VS vasculature (Fig. 1F).

Acidification-induced Ca^{2+} excitation of VS astrocytes is unlikely to be secondary to increased activity of local neurons. To minimize neuronal influences, tetrodotoxin (blocker of voltage-activated sodium channels) and muscimol (potent γ-aminobutyric acid type A receptor agonist) were applied. Both drugs were found to silence RTN neurons (the only known type of pH-responsive neurons in this area), but neither drug affected pH-induced $[Ca^{2+}]_i$ responses monitored using *Case12* or Rhod-2 fluorescence (Fig. 1D and fig. S6). Furthermore, activation of RTN chemoreceptor neurons ($n = 11$ neurons) by current injection failed to trigger $[Ca^{2+}]_i$ elevations even in the immediately adjacent astrocytes (fig. S7).

High pH-sensitivity is a distinctive feature of astrocytes residing near the VS. Astrocytes from the cerebral cortex or dorsal brainstem generated no $[Ca^{2+}]_i$ signals in response to acidification (fig. S8). Moreover, low-magnification Rhod-2 imaging throughout the whole brainstem cross-section revealed that chemosensory stimulation evokes Ca^{2+} responses originating

[1]Neuroscience, Physiology, and Pharmacology, University College London, London WC1E 6BT, UK. [2]Department of Physiology and Pharmacology, University of Bristol, Bristol BS8 1TD, UK. [3]Department of Bioengineering, Stanford University, Stanford, CA 94305, USA.

*To whom correspondence should be addressed. E-mail: a.gourine@ucl.ac.uk (A.V.G.); sergey.kasparov@bristol.ac.uk (S.K.)

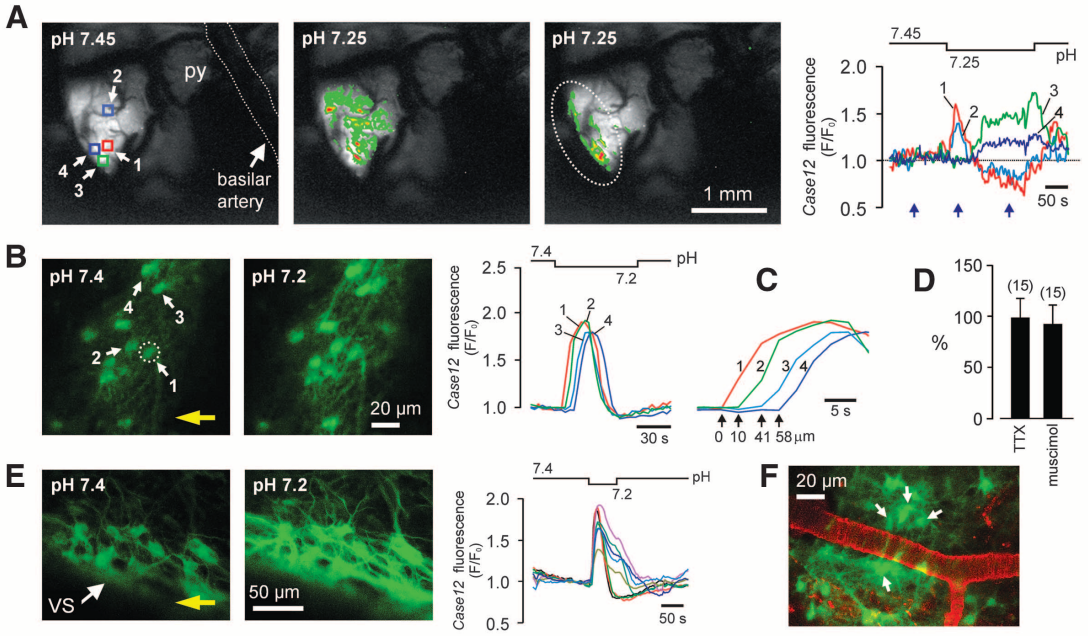

Fig. 1. Astrocytes residing near the VS are exquisitely pH-sensitive. (**A**) In vivo imaging of pH-evoked astrocytic $[Ca^{2+}]_i$ responses in the ventrolateral area of the brainstem surface transduced with AVV-sGFAP-*Case12* in an anesthetized adult rat. (Far right) Changes in VS astrocytic $[Ca^{2+}]_i$ in response to a decrease in pH. (Left) Pseudocolored images were taken at times indicated by arrows. Squares indicate regions of interest. Here and elsewhere, the pH bar shows when the solution with lower pH is reaching and starts leaving the preparation. The dashed line outlines the approximate boundary of the RTN. py, pyramidal tract. (**B**) VS astrocytes identified by means of *Case12* fluorescence in a horizontal slice from an adult rat in which the ventral medulla was transduced with AVV-sGFAP-*Case12*. Acidification induces rapid increases in $[Ca^{2+}]_i$ as determined by changes in *Case12* fluorescence. The two fluorescent images were obtained (left) before and (right) at the peak of $[Ca^{2+}]_i$ response. The circle indicates an astrocyte responding first to pH change in the field of view. The yellow arrow shows the direction of the flow in the chamber. (**C**) Zoomed-in Ca^{2+} transients in order to emphasize the latency differences between responses of individual astrocytes shown in (B). (**D**) No effect of TTX or muscimol on acidification-induced $[Ca^{2+}]_i$ responses in VS astrocytes expressed as percentage of the peak initial response. Numbers of individual astrocytes sampled from three to five separate experiments are given in brackets. (**E**) Acidification-evoked $[Ca^{2+}]_i$ responses in VS astrocytes of organotypic brainstem slice transduced with AVV-sGFAP-*Case12*. The yellow arrow shows the direction of the flow in the chamber. (**F**) VS vasculature visualized with lectin in a horizontal slice prepared from an AVV-sGFAP-*Case12*–transduced rat. Arrows point at pH-responsive astrocytes.

and propagating only near the VS (n = 8 slice preparations) (fig. S9 and movie S4).

Propagation of pH-evoked Ca^{2+} excitation among ventral medullary astrocytes is largely mediated by the actions of adenosine triphosphate (ATP) (SOM text 2.3). A decrease in pH from 7.4 to 7.2 (at constant [HCO_3^-] and nominal P_{CO_2}) triggers sustained ATP release from the VS (peak increase 1.0 ± 0.3 μM, n = 8 horizontal brainstem slice preparations of young adult rats) (Fig. 2A), confirming our previous findings (*20*). Blockade of ATP signaling dramatically diminishes pH-evoked astrocytic responses: In cultured and acute brainstem slices, pH-evoked astrocytic Ca^{2+} responses were abolished in the presence of ATP-hydrolyzing enzyme apyrase (25 U ml^{-1}) (Fig. 2, B and E). Furthermore, ATP receptor antagonists MRS2179 (3 μM), pyridoxalphosphate-6-azophenyl-2',4'-disulfonic acid (PPADS) (5 μM), or 2′,3′-O-(2,4,6-trinitrophenyl) (TNP)–ATP (20 nM) reduced acidification-induced astrocytic $[Ca^{2+}]_i$ signals by 82% (P = 0.005) (Fig. 2C), 80% (P = 0.005), and 83% (P = 0.048), respectively (Fig. 2E). In line with the absence of acidification-induced $[Ca^{2+}]_i$ responses in Ca^{2+}-free medium (Fig. 2E and fig. S10), this pharmacological profile suggests the involvement of ionotropic ATP receptors (SOM text 2.4).

In response to a decrease in pH, the VS astrocytes spread Ca^{2+} excitation partially via gap junctions and predominantly through exocytotic release of ATP (SOM text 2.3). Gap junction blocker carbenoxolone at high concentration (100 μM) was only partially effective in reducing astrocytic $[Ca^{2+}]_i$ responses (by 43%; P = 0.001) (Fig. 2E and fig. S11). In contrast, brefeldine A (vesicular trafficking inhibitor; 50 μM) or bafilomycin A (vesicular H^+-ATPase inhibitor; 2 μM) both effectively abolished acidification-induced Ca^{2+} excitation of VS astrocytes (Fig. 2, D and E). Neither brefeldine A nor bafilomycin A prevented responses of VS astrocytes to applied ATP (Fig. 2D), indicating that astrocytic reactivity to ATP was not affected by these compounds.

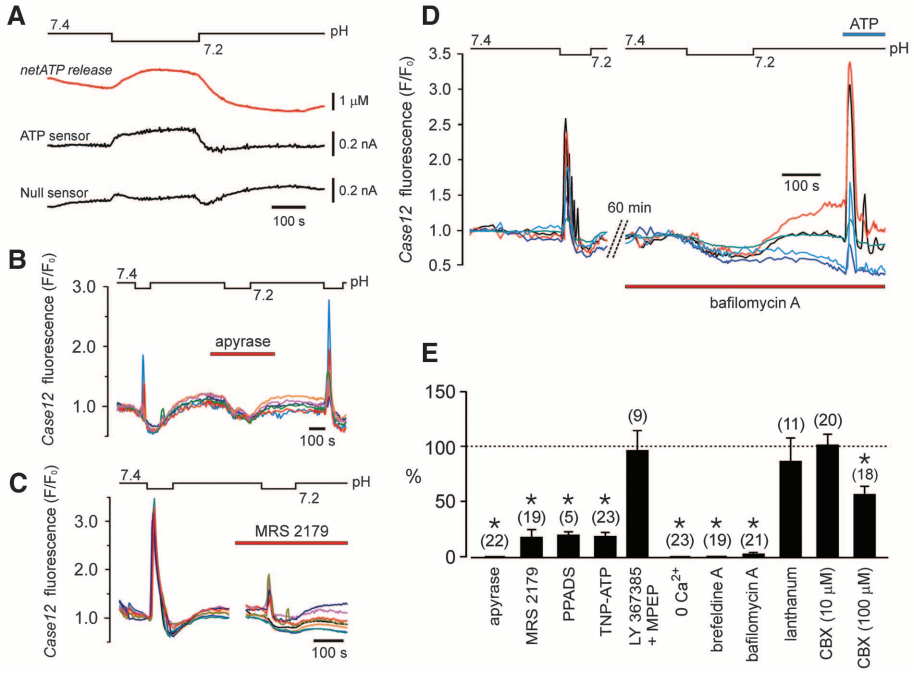

Fig. 2. Exocytotic release of ATP propagates pH-induced Ca^{2+} excitation among VS astrocytes. (**A**) A 0.2-unit decrease in pH induces sustained ATP release from the VS as detected with biosensors placed on the pia mater in horizontal slices prepared from adult rats. "netATP" trace represents the difference in signal between ATP and null (control) sensor currents. (**B**) Apyrase abolishes pH-evoked $[Ca^{2+}]_i$ responses in VS astrocytes. Traces illustrate the effects of apyrase on pH-induced changes in *Case12* fluorescence of six individual astrocytes (adult rat slice preparation). The decrease in signal is due to acidification-induced quenching of *Case12* fluorescence. (**C**) The effect of MRS2179 on acidification-induced $[Ca^{2+}]_i$ responses of eight individual VS astrocytes (organotypic brainstem slice). (**D**) Bafilomycin A abolishes pH-evoked Ca^{2+} excitation of VS astrocytes (five individual astrocytes in slice preparation of an adult rat). (**E**) The effects of apyrase, ATP receptor antagonists, $mGlu_{1a}$ and $mGlu_5$ receptor antagonists (LY367385 and MPEP, 100 μM each), blockers of pannexin/connexin hemichannels and gap junctions lanthanum (100 μM) and carbenoxolone (CBX), or inhibitors of exocytotic mechanisms on acidification-induced $[Ca^{2+}]_i$ responses in VS astrocytes expressed as the percentage of the initial response. Numbers of individual astrocytes sampled from three to five separate experiments are given in brackets (*P < 0.05).

Released ATP also links astrocytic excitation to the increased activity of medullary chemoreceptor neurons. The RTN, which is adjacent to the VS, has been advocated to play a key role in central respiratory chemosensitivity (*21*) (SOM text 2.7). RTN neurons respond to changes in pH, reside within the marginal VS glial layer or have extensive dendritic projections to it, project to the respiratory network, and stimulate breathing upon activation (*21*, *22*).

RTN neurons characteristically express transcription factor Phox2b and were fluorescently labeled with enhanced green fluorescent protein (EGFP) in organotypic slices by using an adenoviral vector with PRSx8 promoter [Phox2b-activated promoter (*23*)] (Fig. 3A). A decrease in pH led to a reversible depolarization of all recorded RTN neurons (n = 8 neurons) (Fig. 3, A and B). Caudally located catecholaminergic C1 neurons were insensitive to pH (fig. S12). MRS2179 (10 μM; n = 8 neurons) (Fig. 3, A and B) or apyrase (25 U ml^{-1}; n = 3 neurons) (fig. S13) had no effect on resting membrane potential but markedly reduced pH-evoked depolarizations of RTN neurons (P = 0.014 and P = 0.04, respectively). In a separate experiment, $[Ca^{2+}]_i$ responses of RTN neurons were visualized by using a genetically encoded Ca^{2+} sensor TN-XXL (*24*) expressed under PRSx8 promoter control (Fig. 3C). Again, acidification-induced $[Ca^{2+}]_i$ elevations in RTN neurons were suppressed by MRS2179 (3 μM, n = 9 neurons, P = 0.008) (Fig. 3, C and D), confirming that their pH-sensitivity is largely mediated by prior release of ATP (SOM text 2.7).

In order to mimic Ca^{2+} excitation of astrocytes, we generated an adenoviral vector in which a mutant of the light-sensitive channelrhodopsin-2 [ChR2-H134R (*25*, *26*)] is fused to a far red-shifted fluorescent protein Katushka1.3 (*27*) and expressed by using enhanced GFAP promoter (Fig. 3E and fig. S14) (*19*). In primary cultures and in brainstem slices of adult rats, astrocytes transduced with this construct displayed robust increases in $[Ca^{2+}]_i$ in response to 470 nm light (Fig. 3F and figs. S15 to S17).

Optogenetic activation of VS astrocytes transduced with AVV-sGFAP-ChR2(H134R)-Katushka1.3 in organotypic brainstem slices triggered immediate ATP release (fig. S18) and evoked long-lasting (28 ± 9 min) depolarizations of all recorded DsRed-labeled RTN neurons (n = 13 neurons) (Fig. 3, G to I). These depolarizations were reversibly prevented in the presence of MRS2179 (10 μM) (P = 0.002) (Fig. 3, H and I).

To determine the functional importance of Ca^{2+} excitation of VS astrocytes, we conducted experiments in anesthetized, vagotomized, and artificially ventilated rats transduced with AVV-sGFAP-ChR2(H134R)-Katushka1.3 in the ventral areas of the brainstem. The VS was exposed, and phrenic nerve activity was recorded so as to monitor central respiratory drive. Unilateral illumination (445 nm) of the transduced side of the

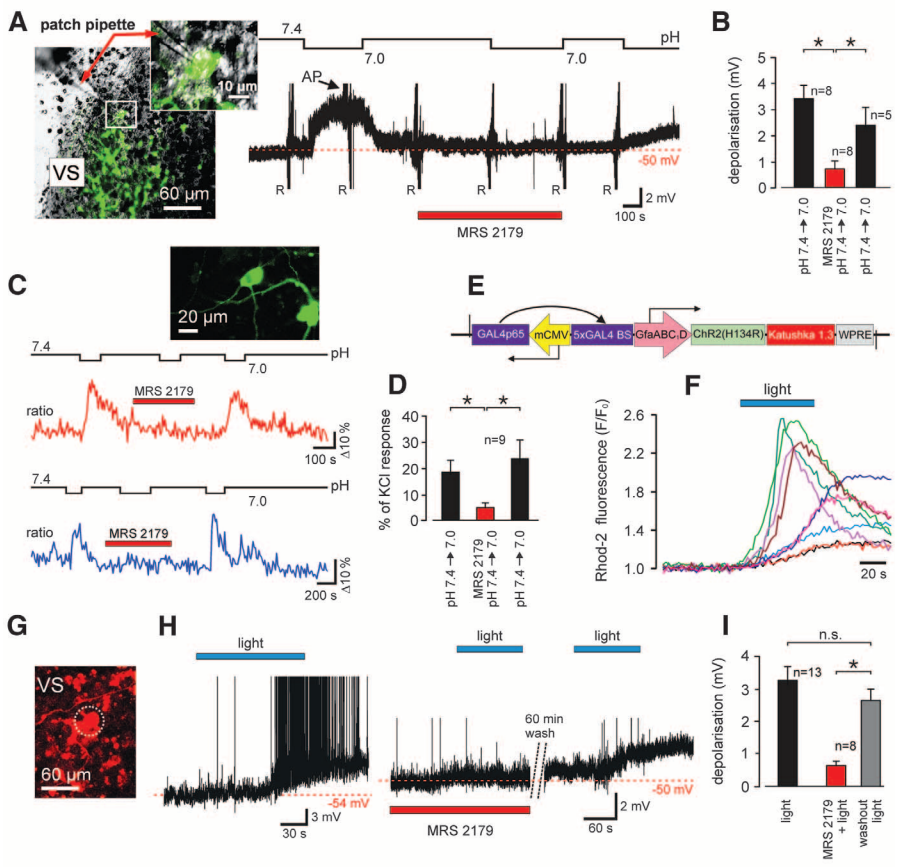

Fig. 3. ATP mediates responses of chemoreceptor neurons to decreases in pH or evoked by selective light-induced Ca^{2+} excitation of adjacent astrocytes. (**A**) (Left) Image of the ventral aspect of an organotypic brainstem slice showing EGFP-labeled Phox2b-expressing RTN neurons, one of which is patch clamped. (Right) Time-condensed record of the membrane potential of an RTN neuron responding to acidification in the absence and presence of MRS2179. AP, action potentials (truncated); R, resistance tests using current pulses. (**B**) Summary of MRS2179 effect on pH-evoked depolarizations in RTN neurons. (**C**) Effect of MRS2179 on acidification-induced $[Ca^{2+}]_i$ responses of RTN neurons from two different experiments (ratiometric imaging using TN-XXL). (Inset) RTN neurons expressing TN-XXL. (**D**) Summary data showing significant effect of MRS2179 on pH-evoked $[Ca^{2+}]_i$ responses of RTN neurons. (**E**) Layout of AAV-sGFAP-ChR2(H134R)-Katushka1.3. (**F**) Primary astrocytes displaying increases in $[Ca^{2+}]_i$ in response to 470 nm light. (**G**) Ventral aspect of the organotypic slice showing a recorded DsRed2-labeled RTN neuron surrounded by ChR2(H134R)-Katushka1.3–expressing astrocytes. (**H**) Membrane potential of two different RTN neurons illustrating their responses to light activation of adjacent ChR2(H134R)-expressing astrocytes in the (left) absence, (middle) presence, or (right) after washout of MRS2179. (**I**) Effects of MRS2179 on depolarizations of RTN neurons evoked by optogenetic activation of neighboring astrocytes (*$P < 0.05$).

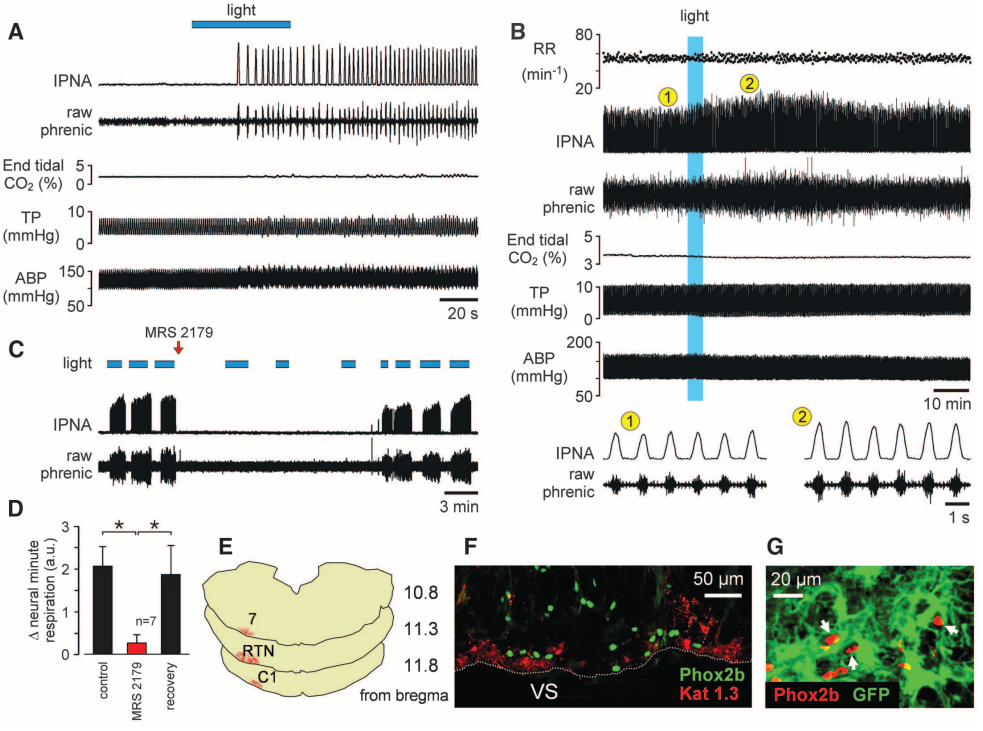

Fig. 4. Optogenetic activation of VS astrocytes stimulates breathing in vivo. (**A**) Unilateral photostimulation of VS astrocytes expressing ChR2(H134R)-Katushka1.3 is sufficient to trigger respiratory activity from hypocapnic apnea in an anesthetized rat. Hypocapnic apnea was induced by means of mechanical hyperventilation to reduce arterial levels of P_{CO_2}/$[H^+]$ below the apneic threshold. IPNA, integrated phrenic nerve activity; TP, tracheal pressure; ABP, arterial blood pressure. (**B**) Lasting effect of light activation of VS astrocytes in an animal breathing normally. RR, respiratory rate. (1) and (2) indicate expanded traces of phrenic nerve activity before and after photostimulation of VS astrocytes. (**C**) Time-condensed record illustrating effects of repeated stimulations of VS astrocytes on phrenic nerve activity before and after a single application of MRS2179 (100 μM, 20 μl) on the VS. Spontaneous recovery of the response over time can be seen. (**D**) Summary data of MRS2179 effect on the increases in neural minute respiration (the product of phrenic frequency and amplitude) evoked by light activation of VS astrocytes (*$P < 0.05$). (**E**) Rostrocaudal distribution of astrocytes expressing ChR2(H134R)-Katushka1.3 in the brainstem of the rat from the experiment shown in (A). 7, facial nucleus; RTN, retrotrapezoid nucleus; C1, catecholaminergic cell group. (**F**) ChR2(H134R)-Katushka1.3 (Kat 1.3) expression in astrocytes is identified by red fluorescence distributed near the VS in close association with Phox2b-immunoreactive neurons (green nuclei). Shown is the coronal brainstem section. (**G**) Phox2b-expressing chemoreceptor RTN neurons (red nuclei) embedded in the astrocytic network (astrocytes were transduced with *Case12* in this example so as to reveal their morphology).

VS triggered robust respiratory activity from hypocapnic apnea in all eight animals tested (Fig. 4A and movie S5). An increase in phrenic nerve amplitude was also observed after optogenetic activation of VS astrocytes in six animals breathing normally ($P < 0.01$) (Fig. 4B). MRS2179 prevented the respiratory effects of optogenetic stimulation of astrocytes ($n = 7$ rats, $P = 0.006$) (Fig. 4, C and D). No responses were induced after illumination of the brainstem side not expressing the transgene. Histological analysis of the areas that stimulation of which evoked increases in breathing (Fig. 4E) revealed close association of transduced astrocytes with the VS and Phox2b-expressing neurons (Fig. 4F).

Although previous reports suggested that astrocytes could potentially be important for chemoreception (*28*, *29*), it was generally believed that central respiratory chemosensory function is a property of one or several highly specialized neuronal populations located in the medulla oblongata and pons. Although our data do not exclude the existence of such neurons, we demonstrate that astrocytes may as well fulfill an equivalent role. Indeed, astrocytes are intimately associated with blood vessels supplying the lower brainstem: Surface pial arteries rest on glia limitans, whereas penetrating arterioles and capillaries are enwrapped by astrocytic end-feet (fig. S3). Therefore, astrocytes anatomically are ideally positioned to monitor the composition of the arterial blood entering the brain and integrate this information with $P_{CO_2}/[H^+]$ levels of brain parenchyma. They have the ability to sense physiological changes in $P_{CO_2}/[H^+]$ and then impart these changes to the respiratory neuronal network to modify breathing patterns and adjust lung ventilation accordingly [although the initial chemosensory event linking a decrease in pH with VS astrocytic $[Ca^{2+}]_i$ response as yet remains unknown (SOM text 2.6)]. This identifies astroglia as an important component of one of the most fundamental mammalian homeostatic reflexes and provides direct evidence for an active role of astrocytes in functionally relevant information processing in the central nervous system.

References and Notes

1. R. D. Fields, B. Stevens-Graham, *Science* **298**, 556 (2002).
2. M. Zonta *et al.*, *Nat. Neurosci.* **6**, 43 (2003).
3. T. Takano *et al.*, *Nat. Neurosci.* **9**, 260 (2006).
4. P. G. Haydon, G. Carmignoto, *Physiol. Rev.* **86**, 1009 (2006).
5. C. Iadecola, M. Nedergaard, *Nat. Neurosci.* **10**, 1369 (2007).
6. G. R. Gordon, H. B. Choi, R. L. Rungta, G. C. Ellis-Davies, B. A. MacVicar, *Nature* **456**, 745 (2008).
7. M. M. Halassa, T. Fellin, H. Takano, J. H. Dong, P. G. Haydon, *J. Neurosci.* **27**, 6473 (2007).
8. E. A. Bushong, M. E. Martone, Y. Z. Jones, M. H. Ellisman, *J. Neurosci.* **22**, 183 (2002).
9. J. Kang, L. Jiang, S. A. Goldman, M. Nedergaard, *Nat. Neurosci.* **1**, 683 (1998).
10. O. Pascual *et al.*, *Science* **310**, 113 (2005).
11. X. Wang *et al.*, *Nat. Neurosci.* **9**, 816 (2006).
12. P. Jourdain *et al.*, *Nat. Neurosci.* **10**, 331 (2007).
13. J. Schummers, H. Yu, M. Sur, *Science* **320**, 1638 (2008).
14. C. Henneberger, T. Papouin, S. H. Oliet, D. A. Rusakov, *Nature* **463**, 232 (2010).
15. M. M. Halassa *et al.*, *Neuron* **61**, 213 (2009).
16. E. A. Souslova *et al.*, *BMC Biotechnol.* **7**, 37 (2007).
17. Materials and methods are available as supporting material on *Science* Online.
18. H. H. Loeschcke, *J. Physiol.* **332**, 1 (1982).
19. B. Liu, J. F. Paton, S. Kasparov, *BMC Biotechnol.* **8**, 49 (2008).
20. A. V. Gourine, E. Llaudet, N. Dale, K. M. Spyer, *Nature* **436**, 108 (2005).
21. D. K. Mulkey *et al.*, *Nat. Neurosci.* **7**, 1360 (2004).
22. S. B. Abbott *et al.*, *J. Neurosci.* **29**, 5806 (2009).
23. D. Y. Hwang, W. A. Carlezon Jr., O. Isacson, K. S. Kim, *Hum. Gene Ther.* **12**, 1731 (2001).
24. M. Mank *et al.*, *Nat. Methods* **5**, 805 (2008).
25. V. Gradinaru *et al.*, *J. Neurosci.* **27**, 14231 (2007).
26. In the mutants, amino acids were substituted at certain locations; for example, H134R indicates that histidine (H) at position 134 was replaced by arginine (R).
27. D. Shcherbo *et al.*, *Biochem. J.* **418**, 567 (2009).
28. Y. Fukuda, Y. Honda, M. E. Schläfke, H. H. Loeschcke, *Pflugers Arch.* **376**, 229 (1978).
29. N. A. Ritucci, J. S. Erlichman, J. C. Leiter, R. W. Putnam, *Am. J. Physiol.* **289**, R851 (2005).

30. We are grateful to The Wellcome Trust (grant 079040) and British Heart Foundation for financial support. A.V.G. is a Wellcome Trust Senior Research Fellow.

Supporting Online Material

www.sciencemag.org/cgi/content/full/329/5991/571/DC1
Materials and Methods
SOM Text
Figs. S1 to S26
Table S1
References
Movies S1 to S5

9 April 2010; accepted 25 June 2010
10.1126/science.1190721